Universidad de Alcalá
BIBLIOTECA

Document downloaded from the institutional repository of the University of Alcala: https://ebuah.uah.es/dspace/

This is a postprint version of the following published document:

García-Iriepa, C. et al. (2013) 'Chiral Hydrogen Bond Environment Providing Unidirectional Rotation in Photoactive Molecular Motors', The journal of physical chemistry letters, 4(9), pp. 1389–1396.

Available at https://doi.org/10.1021/jz302152v

© 2013 American Chemical Society

Universidad de Alcalá

(Article begins on next page)

This work is licensed under a

Creative Commons Attribution-NonCommercial-NoDerivatives 4.0 International License.

Chiral Hydrogen Bond Environment Providing Unidirectional Rotation in Photoactive Molecular Motors

Cristina García-Iriepa†‡, Marco Marazzi†, Felipe Zapata†, Alessio Valentini†, Diego Sampedro*‡, and Luis Manuel Frutos*†

† Departamento de Química Física, Universidad de Alcalá, E-28871 Alcalá de Henares, Madrid, Spain
‡ Departamento de Química, Centro de Investigación en Síntesis Química (CISQ), Madre de Dios 51, E-26006 Logroño, Spain
*E-mail: diego.sampedro@unirioja.es. Fax: +34 941 299 621. Tel: +34 941 299 647 (D.S.); luisma.frutos@uah.es. Fax: +34 91 885 4639. Tel: +34 91 885 2512 (L.M.F.).

Abstract

Generation of a chiral hydrogen bond environment in efficient molecular photoswitches is proposed as a novel strategy for the design of photoactive molecular motors. Here, the following strategy is used to design a retinal-based motor presenting singular properties: (i) a single excitation wavelength is needed to complete the unidirectional rotation process (360°); (ii) the absence of any thermal step permits the process to take place at low temperatures; and (iii) the ultrafast process permits high rotational frequencies.

Construction of molecular devices with specific atomic-level properties has been a fundamental aim of nanotechnology in the last decades, as demonstrated by the design of molecular switches (1, 2) and motors, (3) regular two/three-dimensional rotor arrays, (4) nanocars, (5) gyroscopes, (6) and so forth. Among these devices, molecular motors are of special interest as the input energy is converted into a controlled motion (unidirectional rotation) that plays an important role in both artificial and biological systems. Examples of Nature's molecular motors are the ATP synthase, kinesine, myosine, and flagellar motors in bacteria, all of them being essential for life. (7) Furthermore, artificial molecular motors have been proposed as crucial parts of molecular-level machines, mimicking biological systems by performing a specific function. The most suitable approach for chemists to construct molecular motors is the bottom-up approach, that is, starting from atoms or small building blocks. (8)

The design of efficient molecular motors should satisfy the following criteria: the energy supplied has to be transformed into a unidirectional repetitive rotary movement of 360° (i.e. mechanical work), and repetition of a high number of cycles has to be ensured (i.e., fatigue resistance). (9) The unidirectionality can be achieved by a protein or chiral environment (such as a protein surrounding (10) or a helical structure (11)). For novel applications (microscopic movement, control of

macroscopic properties of materials, supramolecular organization and assemblies), (12) these devices are required to perform rotation at a considerable speed with high quantum yields. In contrast to Brownian, (13) electrically, (14) or chemically (15) driven motors, photoactivated ones are greatly profitable due to the manifest advantages of light as the energy supply. (11b, 16) Among these types of devices, the ones reported by Feringa et al., based on a helical structure, are the most studied. (11) They present high quantum yields and need four steps (two photochemical and two thermal) to complete a cycle. Whereas the photochemical steps (Z–E photoisomerizations around a carbon–carbon double bond) are extremely fast, the thermal ones are rate-limiting, decreasing the rotational frequency of these devices. Further structural and electronic modifications have enhanced this weakness, leaving in any case the thermal isomerization steps as the bottleneck of the overall mechanism. (11b, 17) Indeed, further theoretical studies have offered new insights to reduce or eliminate the thermal helix inversion steps of the overall mechanism. (18)

The approach presented here for the rational design of photoactive molecular motors is based on the use of an efficient photoactive molecular switch as the starting unit, in which a chiral environment is introduced via hydrogen bonds in order to obtain a molecular motor. Indeed, the complete rotation of this novel molecular motor is achieved only by two photochemical steps (no thermal steps are involved in the mechanism).

Photoactive molecular switches undergo Z–E photoisomerization around a given C═C, yielding the conversion between both stable states (Z and E). In order to control the photoreactivity of Z–E photoswitches, a general design strategy consists of blocking all but one double bond of the system by including them in rings of different size. Here, we use a molecular system exhibiting these characteristics, where only the central C═C bond linking two unsaturated rings is able to undergo Z–E photoisomerization. In this way, starting from a Z–E photoswitchable molecule with two equivalent ground-state minima (see Figure 1A), a chiral environment is introduced by including two hydroxyl groups linked to chiral carbon atoms, which permits formation of one hydrogen bond between the amino group and one of the two hydroxyl groups. Because the hydroxyl groups are linked to a chiral carbon atom, we refer to this chemical ensemble as a chiral hydrogen bond environment (see Figure 1B). This chiral environment induces a guided pretwist around the C═C central bond in the ground state, leading to a single stable minimum on the ground state, which ultimately drives the unidirectional rotation in the excited state.

Figure 1

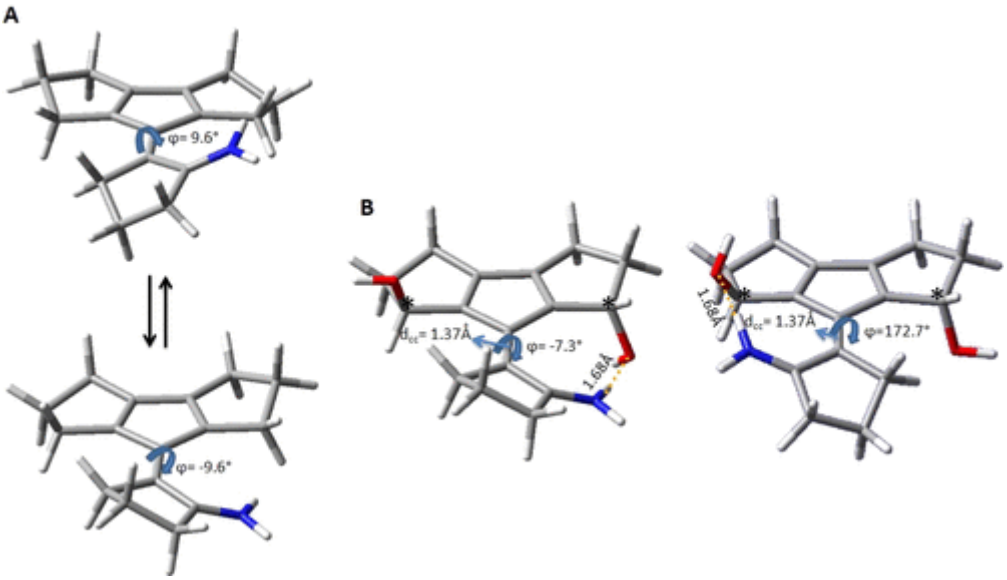

Figure 1. (A) Structure of the starting molecular photoswitch in its two possible conformations. Due to the same population for both isomers in the ground state, the system behaves as a photoswitch with no unidirectional rotation. (B) The corresponding derived molecular motor where the chiral hydrogen bond environment is introduced via −OH groups; the two symmetrically equivalent ground-state structures are shown, tailoring the two minima structures of the complete photocycle. Chiral carbon atoms with −OH are marked.

On the one hand, planar Z–E chromophores, as a retinal Schiff base photoswitch in gas and liquid phase, exhibit a $^1(\pi,\pi^*)$ photoactive excited electronic state. (19) Excitation to this electronic state is usually related to a vibrational excess (20) in the stretching modes involving the π system, provoking a bond length alternation of the conjugated backbone in the excited state. This vibrational energy is eventually transferred to the Z–E torsion mode involving molecular symmetry breaking and inducing the torsion in the excited state (i.e., stretching and torsion modes are not coupled in the case of strictly planar systems). The vibrational energy transfer takes place in many stretching cycles due to the lack of stretching–torsion coupling, which increases as the torsion becomes higher. (19a, 21) Finally, a conical intersection (CI) with the ground state allows the torsion to be completed. In this situation, the evolution of the torsion coordinate in the excited state is not controlled, and the system can equally evolve in both possible directions (clockwise and counterclockwise). This noncontrolled torsion direction characterizes Z–E photoactive molecular switches.

Conversely, for nonplanar Z–E photoactive molecular switches, the existing coupling between stretching and torsion modes (i.e., the second derivative cross term) provokes the rapid flow of vibrational energy from

excited stretching modes to torsional modes in the electronic excited state, contrary to the above-discussed planar systems. This is the case of retinal in rhodopsin, where the unidirectional rotation is guided especially by the surrounding amino acids of the opsin pocket, which provide a chiral environment. (10, 22) This environment not only guides the rotation in the excited state but also accelerates the rotation due to the increase of the stretching–torsion coupling, making the Z–E isomerization process take place on the femtosecond time scale. (22, 23)

The inclusion of the above-mentioned chiral hydrogen bond environment in the studied molecular photoswitch (see Figure 1B) modifies its force field, breaking the symmetry of the potential energy surfaces (PESs) along the torsion coordinate, giving rise to a single isomer instead of two isomers of the preceding photoswitch. This, in turn, as will be shown, ultimately permits the unidirectional rotation of the system.

In this regard, it is convenient to analyze the PESs (ground and optically bright states) corresponding to three different cases, planar photoswitches, nonplanar photoswitches, and the derived photoactive molecular motors, in order to realize what the initial rotation direction is after electronic excitation. Planar Z–E photoswitches present symmetrical PES profiles along the torsion coordinate; therefore, torsion is not controlled in any way, and two possible equivalent relaxation paths are accessible (see Figure 2A). Nevertheless, a photoswitch can exhibit nonplanarity, as is the case of the system studied here (see Figure 1A). For nonplanar switches, two equivalent conformations for each Z and E isomer may exist, and even if the torsion for each conformer were unidirectional, the equivalent population of both isomers in the ground state makes the system behave as a photoswitch (see Figure 2B). On the contrary, unidirectional rotation present in Z–E photoactive molecular motors is related to nonsymmetrical PESs in the excited and ground states along the torsion coordinate, with a single ground-state minimum and the rotation of the system being unidirectionally initiated in the excited state (see Figure 2C).

Figure 2

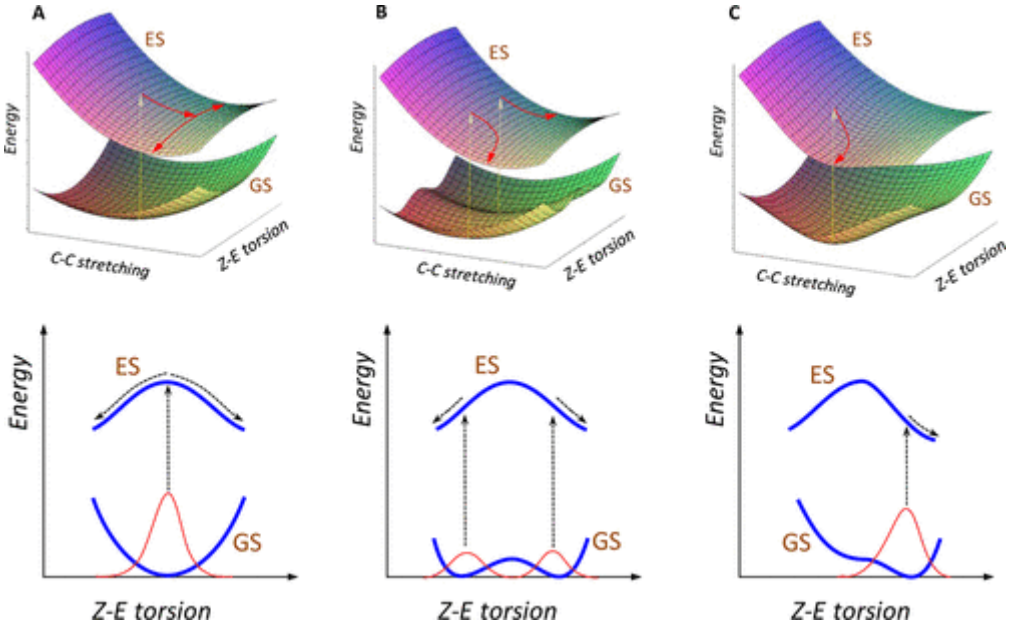

Figure 2. Schematic ground-state (GS) and excited-state (ES) PESs (up) and the corresponding distribution population on the ground state (down) for three different systems: (A) A planar photoswitch presenting a vanishing coupling between central bond torsion and stretching coordinates. Two rotation directions are possible in this case, and therefore, two minimum-energy paths bifurcate in the excited state at a transition state (noncontrolled rotational direction). (B) A nonplanar photoswitch showing two equivalent minima on the ground state, each one related to opposite rotation directions. (C) A photoactive molecular motor where the chiral hydrogen bond environment breaks the symmetry of the PES in both ground and excited states. The coupling between central bond torsion and stretching coordinates is not vanishing, inducing the torsion in a specific direction (controlled rotational direction).

In order to ensure this unidirectional rotation, we generate a chiral hydrogen bond environment within a molecular photoswitch structure. This can be formally seen as a conversion from a photoswitch (Figure 1A) to a molecular motor (Figure 1B), which can be understood in terms of PESs. In contrast for the photoswitch (Figure 2B), there is no preference for the direction of rotation in the excited state; in chiral environments induced by a hydrogen bond, the symmetry is already broken in the ground state, which provokes the stabilization of the system along a specific torsion, resulting in a unidirectional rotation in the excited state (see Figure 2C).

Moreover, as will be shown, the strength of the hydrogen bond of the studied system is enough to correctly drive the torsion on the excited state but not so strong to block the rotation in this state, generating an intermediate and therefore quenching the process. Thus, the strength of

the hydrogen bond could be critical in the design of an efficient motor, and it should be tuned for an optimal performance.

It should be noted that this design of a molecular motor with two symmetrically equivalent structures (for the initial and the 180° rotated isomers) would allow a continuous unidirectional movement using only a specific wavelength source. As a drawback, the experimental characterization of the molecular device would be difficult. From a practical point of view, this difficulty could be overcome through the modification of the basic design by including a group that could break the symmetry without altering the functioning of the motor.

For the study of the photochemical and photophysical properties of the proposed molecular motor, the multiconfigurational CASPT2//CASSCF (24) methodology has been employed with a 6-31G* basis set. The active space chosen is composed of all of the π and π* orbitals (eight electrons in eight orbitals), therefore including all of the energy low-lying $^1(\pi,\pi^*)$ excited states. The stationary points have been determined by using analytical energy gradients computed at the CASSCF level and characterized by numerical frequency calculations at the same level of theory. Minimum energy paths (MEPs) were computed for the determination of the photoreaction mechanism, and crossings between electronic states were characterized by determining the derivative coupling (DC) and gradient difference (GD) vectors. (25) All calculations have been performed with MOLCAS 7.6 (26) and the Gaussian 09 (27) suite of programs.

The UV–visible absorption spectrum is characterized by a low-lying optically bright π,π* excited state, S_2, exhibiting a dominant monoexcitation configuration with a large participation of the central carbons of the double bond in both, the occupied and the virtual orbitals involved in the excitation. The shape of these orbitals clearly indicates the rupture of the central carbon–carbon double bond in the excited state and the consequential favored torsion around this bond. The S_3 state has a similar electronic nature, showing a larger contribution of the configuration described by the $^1(\pi,\pi^*)$ central π double bond excitation. In fact, the $S_0 \rightarrow S_2$ and $S_0 \rightarrow S_3$ vertical excitations are close in energy (280 and 291 nm, respectively) with similar oscillator strengths (0.32 and 0.35, respectively).

Excitation of the system to the brightest states (S_3 and S_2) leads to similar profiles along the MEP, characterized by a steep energy variation along the increasing carbon–carbon central bond distance. This coordinate is significantly coupled with the torsion around the same bond in the direction guided by the hydrogen bond (see Figure 3). The coupling

between the central bond stretching and torsion is essential, as discussed above, in controlling the unidirectional rotation. This allows the system to transfer the excitation energy, initially located in the stretching coordinates, to the torsional coordinate, inducing unidirectional rotation. Moreover, inverse (i.e., counterclockwise) rotation is not feasible due to the large energy barrier as a result of a double effect opposing this rotation, that is, hydrogen bond breaking and reversion of the already twisted torsion in the excited state (see the Supporting Information for details). The latter effect can be clarified by analyzing the excited-state PES along the torsional coordinate; for symmetric systems (see Figure 2A), the highest excited-state energy corresponds to a planar photoswitch, and torsion around this coordinate makes the energy decrease as a result of diradical repulsion; therefore, if the system is initially twisted at some degree of torsion, the reversion toward the planarity is energetically demanding, making the counterclockwise rotation unfavorable.

Figure 3

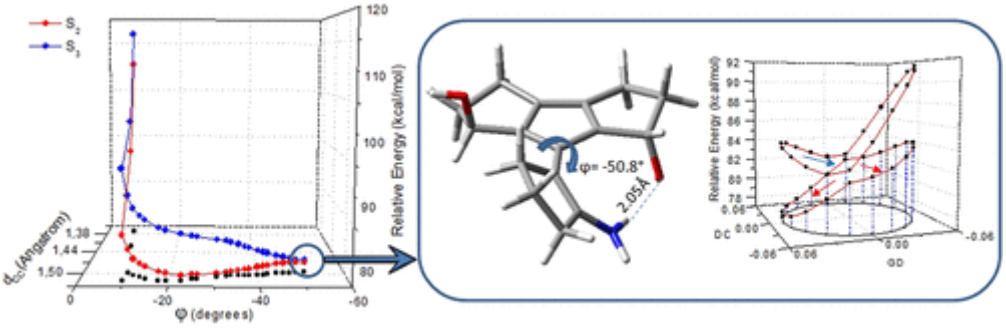

Figure 3. S_3 and S_2 energies along the MEP on S_3 after vertical excitation, represented as a function of the central bond torsion and stretching coordinates (left). The S_3/S_2 conical intersection structure is shown, as well as the S_3 and S_2 energy profiles around the tip of the conical intersection for a loop defined on the branching plane (28) with a 0.05 Åradius. The decay paths from S_3 (blue arrow) to S_2 (red arrows) are indicated.

Relaxing along the torsional mode in S_3, the system reaches a low-sloped S_3/S_2 CI at ~−51° of torsion with a vibrational excess of ~22 kcal/mol. After decay to S_2, the system continues rotating because of a significant impulse along the rotation direction. It should be noted that no intermediate is found in the relaxation process, indicating that the hydrogen bond strength is large enough to guide the torsion after excitation but not so strong to block the rotation on the excited state.

The S_3/S_2 CI is characterized by a NH···O distance of ~2.0 Å. Once this point is reached, the system minimizes its energy by following two different bifurcating paths. The first one reaches a minimum-energy structure at 13 kcal/mol (CASPT2 level) below the S_3/S_2 CI, from where a

low-lying transition state (3.8 kcal/mol at the CASPT2 level) permits it to continue the torsional process started in S_3. The second path directly continues the torsion started in S_3, breaking almost completely the hydrogen bond (see Figure 4). The linear impulse of the nuclei once it reaches the S_3/S_2 CI is expected to be enough to drive the torsion when following both paths, similarly to some highly efficient Z–E photoisomerizing systems like retinal in rhodopsin proteins. (7c, 19a, 29)

Figure 4

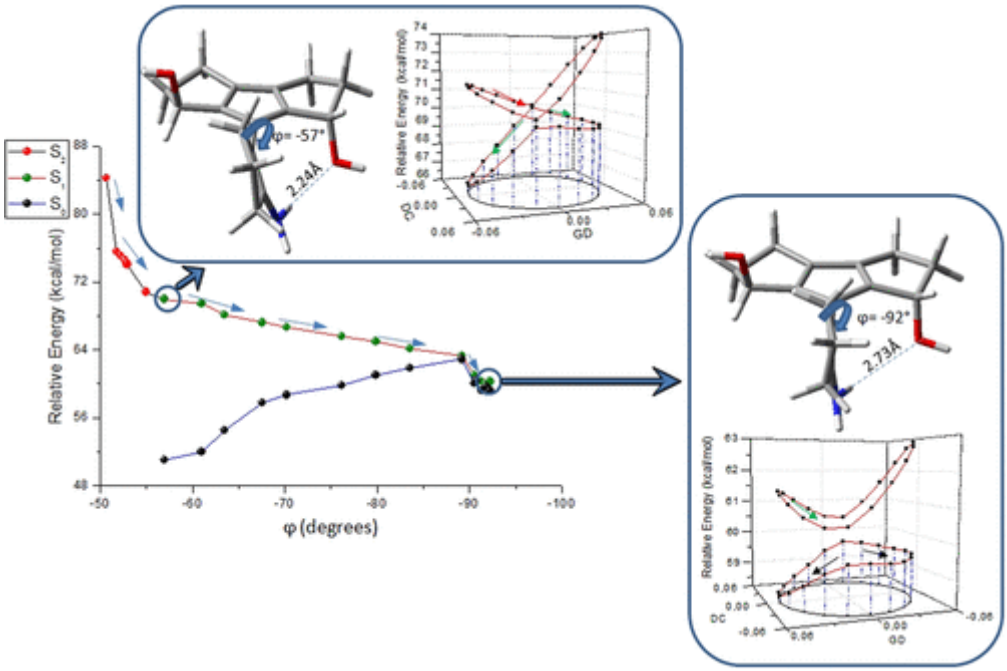

Figure 4. S_2, S_1, and S_0 energy profiles represented along the torsion coordinate for the two MEPs starting at the S_3/S_2 and S_2/S_1 conical intersections. The molecular structures of the conical intersections are displayed, showing, respectively, a very weak and a formally broken hydrogen bond, with central bond torsions of ∼−57 and −92°. The loop around the CI within the branching plane shows the topology of the CI; two possible paths are available for both CIs in the lower surface (S_1 and S_0), as shown by arrows, corresponding to torsion completion or abortion.

Relaxing along the increasing torsion S_2 pathway, the S_2 and S_1 states become rapidly degenerate in energy (see Figure 4). The crossing region between S_2 and S_1 states is reached when the torsion angle is ∼−55°, with the NH···O hydrogen bond formally broken (2.24 Å). These S_2/S_1 CIs enhance the rotational motion, permitting the evolution of the system in the S_1 state, where the rotation is fulfilled at ∼−92° (see Figure 4). At this point, the system intersects a third region of energy degeneration (the S_1/S_0 CI crossing region) that funnels the system into the ground state. The topology of these CIs is similar to those already described in many other Z–E photoisomerization processes. (19a, 21, 29b, 30) From photon absorption to the S_1/S_0 CI, a total energy of ∼43 kcal/mol (at the CASPT2

level) has been converted into vibrational excess mostly located into the torsional mode, resulting in almost twice the energy required for retinal isomerization in rhodopsin. (22)

From this last state crossing, the molecule can evolve along two different paths on the ground state, the first one completing the torsion and the second one aborting the rotation and recovering the initial structure (see the Supporting Information for more details). In both cases, the same initial structure is recovered due to the symmetric arrangement of the two equivalent hydrogen bonds; in the first case, the rotation is completed up to 180°, and in the second case, the rotation is aborted.

The resulting structure after 180° rotation is equivalent to the initial configuration. Therefore, the same rotational process can be fulfilled by absorption of a second photon, completing a 360° cycle by applying a monochromatic UV source with the corresponding wavelength. Moreover, as has been shown, there are no intermediates along the rotational path; therefore, the process is expected to be ultrafast. In addition, the large vibrational excess along the MEPs involving mainly the rotational coordinates makes the complete cycle process to be expected as highly efficient. Nevertheless, nonadiabatic molecular dynamics (NAMD) simulations are necessary in order to quantitatively predict the efficiency of the process. (31)

In order to provide a description of the photoisomerization dynamics, a single reference trajectory without initial kinetic energy (T = 0 K) has been computed by using Tully's fewest switches algorithm (31a) with decoherence correction (31c, 32) working within MOLCAS. (33) This trajectory closely represents the photochemical behavior of the motor at very low temperatures, that is, in the absence of thermal energy boosting or quenching the isomerization.

From the obtained results, it can be concluded that photoisomerization is an efficient and an ultrafast process. Even without initial kinetic energy, the decay to the ground state is reached in ∼260 fs with a torsion φ of ∼−85° (see Figure 5), and the complete photoisomerization takes place in ∼450 fs with a torsion φ of ∼−190° (see the Supporting Information). The excited-state lifetimes can be estimated from the NAMD simulation; S_3, S_2, and S_1 have approximate lifetimes of ∼150, 90 and 20 fs, respectively. According to the time scale of the photoisomerization (∼0.5 ps), the rotation frequency is in the range of 10^{12} s^{-1} (terahertzs), which is, to our knowledge, the highest documented Z–E photoisomerization frequency of a photoactive artificial molecular motor.

Figure 5

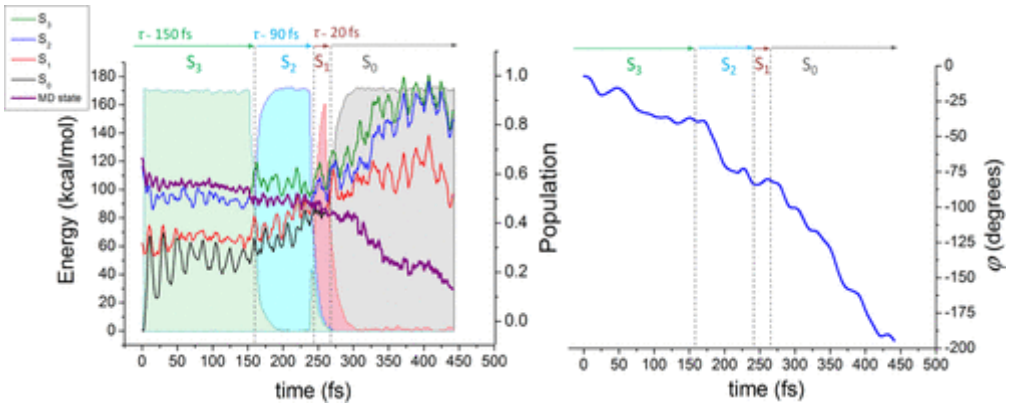

Figure 5. (Left) S_3, S_2, S_1, and S_0 relative energy profiles along the 0 K molecular dynamics simulation (lines, left scale). Populations of every state according to fewest switches algorithm are represented (background, right scale) by dashed filled profiles. Approximate state lifetimes are 150 fs for S_3, 90 fs for S_2, and 20 fs for S_1. S_0 is populated in ~260 fs. (Right) Central torsion angle (φ) evolution along the trajectory.

In order to check the stability of the computed CAS(8,8)/6-31G* trajectory at room temperature, (34) a computationally more affordable 3-21G basis set was employed for the determination of 20 trajectories (see the Supporting Information for details). Although the PESs with both basis sets are qualitatively similar (see the Supporting Information), they present some differences. Specifically, the steepness of the PES along the MEPs is lower for 3-21G than that for 6-31G*. This makes the 3-21G NAMDs slower (larger time scale photoisomerization) and less efficient due to the lesser impulse along the rotational coordinate (e.g., the 0 K NAMD with the 3-21G basis set does not fulfill the photoisomerization, contrary to the 6-31G* trajecotry). Nonetheless, 4 out of 20 trayectories (20%) give rise to the isomerization in a 1.5 ps time window, and more importantly, all of the computed trajectories provide unidirectional rotation after vertical excitation (i.e., counterclockwise rotation is forbidden). These results are in agreement with the 0 K 6-31G* NAMD as well as with the computed MEPs.

In conclusion, in this study, we present a novel concept for the design of photoactive molecular motors, the induction of unidirectional rotation by a chiral hydrogen bond environment. Indeed, molecular photoswitches could be converted into molecular motors by inducing a chiral environment through hydrogen bonds. This kind of design has some novel benefits in comparison to previously reported molecular motors; (i) both Z and E isomers can be designed in order to be structurally identical, as is the case of the present molecular motor (Figure 1). Therefore, a monochromatic light source can be applied to complete the whole photocycle (360°). (ii) Both Z to E and E to Z photoisomerizations take

place in a single step without any energy barrier. Therefore, the process is expected to be ultrafast (taking less than 1 ps) and with radiative or quenching deactivations playing eventually a minor role. (iii) Any efficient molecular photoswitch can be transformed into an efficient photoactive motor by introducing the chiral hydrogen bond environment without modifying the chromophore electronic nature. (iv) The strength of the hydrogen bond(s) is tunable, facilitating the possibility to control the quantum yield of the process.

Supporting Information

Computational details, the excited-state initial rotation direction, molecular dynamics methods and trajectories, absorption spectra, the unidirectional rotation path, CASPT2 energy profiles, and Cartesian coordinates of the most relevant optimized structures are provided. Also given is the NAMD trajectory animation. This material is available free of charge via the Internet at http://pubs.acs.org.

AUTHOR INFORMATION

Corresponding Author *E-mail: diego.sampedro@unirioja.es. Fax: +34 941 299 621. Tel: +34 941 299 647 (D.S.); luisma.frutos@uah.es. Fax: +34 91 885 4639. Tel: +34 91 885 2512 (L.M.F.). Author Contributions The manuscript was written through contributions of all authors. All authors have given approval to the final version of the manuscript.

Notes

The authors declare no competing financial interest.

ACKNOWLEDGMENTS

This research was supported by the Spanish MICINN Grants CTQ2009-07120 and CTQ2011-24800, Spanish MINECO Grant CTQ2012-36966, and the University of Alcalá UAH2011/EXP-041 Grant. C.G.-I. and M.M. are grateful to the UAH for a doctoral fellowship. L.M.F. acknowledges receipt of a “Ramon y Cajal” contract from MEC.

ABBREVIATIONS

CI, conical intersection; CASSCF, complete active space selfconsistent field; CASPT2, complete active space perturbational theory to second order; MEP, minimum energy path; PES, potential energy surface; GS, ground state; ES, excited state; NAMD, nonadiabatic molecular dynamics.

REFERENCES

(1) (a) Feringa, B. L.; van, D. R. A.; Koumura, N.; Geertsema, E. M. Chiroptical Molecular Switches. Chem. Rev. 2000, 100, 1789−1816. (b) Gust, D.; Moore, T. A.; Moore, A. L. Molecular Switches Controlled by Light. Chem. Commun. 2006, 1169−1178. (c) Russew, M.-M.; Hecht, S. Photoswitches: from Molecules to Materials. Adv. Mater. (Weinheim, Ger.) 2010, 22, 3348−3360. (2) García-Iriepa, C.; Marazzi, M.; Frutos, L. M.; Sampedro, D. E/Z Photochemical Switches: Syntheses, Properties and Applications. RSC Adv. 2013, DOI: 10.1039/c2ra22363e. (3) (a) Hernandez, J. V.; Kay, E. R.; Leigh, D. A. A Reversible Synthetic Rotary Molecular Motor. Science 2004, 306, 1532−1537. (b) Kelly, T. R. Progress toward a Rationally Designed Molecular Motor. Acc. Chem. Res. 2001, 34, 514−522. (c) Kelly, T. R.; Silva, R. A.; De, S. H.; Jasmin, S.; Zhao, Y. A Rationally Designed Prototype of a Molecular Motor. J. Am. Chem. Soc. 2000, 122, 6935−6949. (4) (a) Zheng, X.; Mulcahy, M. E.; Horinek, D.; Galeotti, F.; Magnera, T. F.; Michl, J. Dipolar and Nonpolar Altitudinal Molecular Rotors Mounted on an Au(111) Surface. J. Am. Chem. Soc. 2004, 126, 4540−4542. (b) Michl, J.; Sykes, E. C. H. Molecular Rotors and Motors: Recent Advances and Future Challenges. ACS Nano 2009, 3, 1042−1048. (c) Horansky, R. D.; Magnera, T. F.; Price, J. C.; Michl, J. Artificial Dipolar Molecular Rotors. Lect. Notes Phys. 2007, 711, 303−330. (5) (a) Akimov, A. V.; Nemukhin, A. V.; Moskovsky, A. A.; Kolomeisky, A. B.; Tour, J. M. Molecular Dynamics of Surface-Moving Thermally Driven Nanocars. J. Chem. Theory Comput. 2008, 4, 652− 656. (b) Khatua, S.; Guerrero, J. M.; Claytor, K.; Vives, G.; Kolomeisky, A. B.; Tour, J. M.; Link, S. Micrometer-Scale Translation and Monitoring of Individual Nanocars on Glass. ACS Nano 2009, 3, 351−356. (c) Shirai, Y.; Osgood, A. J.; Zhao, Y.; Yao, Y.; Saudan, L.; Yang, H.; Chiu, Y.-H.; Alemany, L. B.; Sasaki, T.; Morin, J.-F.; Guerrero, J. M.; Kelly, K. F.; Tour, J. M. Surface-Rolling Molecules. J. Am. Chem. Soc. 2006, 128, 4854−4864. (6) (a) Godinez, C. E.; Zepeda, G.; Garcia-Garibay, M. A. Molecular Compasses and Gyroscopes. II. Synthesis and Characterization of Molecular Rotors with Axially Substituted Bis[2-(9-triptycyl)ethynyl]- arenes. J. Am. Chem. Soc. 2002, 124, 4701−4707. (b) Dominguez, Z.; Khuong, T.-A. V.; Dang, H.; Sanrame, C. N.; Nunez, J. E.; GarciaGaribay, M. A. Molecular Compasses and Gyroscopes with Polar Rotors: Synthesis and Characterization of Crystalline Forms. J. Am. Chem. Soc. 2003, 125, 8827−8837. (c) Escalante-Sanchez, E.; Rodriguez-Molina, B.; Garcia-Garibay, M. A. Toward Crystalline Molecular Rotors with Linearly Conjugated Diethynyl−Phenylene Rotators and Pentiptycene Stators. J. Org. Chem. 2012, 77, 7428− 7434. (7) (a) Stock, D.; Leslie, A. G. W.; Walker, J. E. Molecular Architecture of the Rotary Motor in ATP Synthase. Science 1999, 286, 1700−1705. (b) Shao, Q.; Gao, Y. Q. On the Hand-over-Hand Mechanism of Kinesin. Proc. Natl. Acad. Sci. U.S.A. 2006, 103, 8072− 8077. (c) Sampedro, D.; Blanco-Lomas, M.; Rivado-Casas, L.; Campos, P. J. Retinal-Based Molecular Machines. In Advances in Biomimetics; George, A., Ed.; InTech: New York, 2011. (d) Kinbara, K.; Aida, T. Toward Intelligent Molecular Machines: Directed Motions of Biological and Artificial Molecules and Assemblies. Chem. Rev. 2005, 105, 1377−1400. (8) Balzni, V.; Venturi, M.; Credi, A. Molecular Devices and Machines: A Journey into the Nano World; John Wiley & Sons: New York, 2003; p 500. (9) Kelly, T. R.; Ed., Molecular Machines. In Topics in Current Chemistry; Springer: New York, 2005; p 236 and 262. (10) (a) Crano, J. C. G.; Guglielmetti, R. J. Organic Photochromic and Thermochromic Compounds; Springer: New York, 1999. (b) Wolken, J. Light Detectors, Photoreceptors, and Imaging Systems in Nature; Oxfors University Press: New York, 1995. (11) (a) Koumura, N.; Zijlstra, R. W.; van Delden, R. A.; Harada, N.; Feringa, B. L. Light-Driven Monodirectional Molecular Rotor. Nature 1999,

401, 152−155. (b) Feringa, B. L. In Control of Motion: From Molecular Switches to Molecular Motors. Acc. Chem. Res. 2001, 34, 504−513. (c) Feringa, B. L. The Art of Building Small: From Molecular Switches to Molecular Motors. J. Org. Chem. 2007, 72, 6635−6652. (12) (a) de Jong, J. J. D.; Hania, P. R.; Pugzlys, A.; Lucas, L. N.; de Loos, M.; Kellogg, R. M.; Feringa, B. L.; Duppen, K.; van Esch, J. H. Light-Driven Dynamic Pattern Formation. Angew. Chem., Int. Ed. 2005, 44, 2373−2376. (b) de Jong, J. J. D.; Lucas, L. N.; Kellogg, R. M.; van Esch, J. H.; Feringa, B. L. Reversible Optical Transcription of Supramolecular Chirality into Molecular Chirality. Science 2004, 304, 278−281. (c) Pijper, D.; Feringa, B. L. Molecular Transmission: Controlling the Twist Sense of a Helical Polymer with a Single LightDriven Molecular Motor. Angew. Chem., Int. Ed. 2007, 46, 3693−3696. (d) Eelkema, R.; Feringa, B. L. Reversible Full-Range Color Control of a Cholesteric Liquid-Crystalline Film by Using a Molecular Motor. Chem.Asian J. 2006, 1, 367−369. (e) Eelkema, R.; Pollard, M. M.; Katsonis, N.; Vicario, J.; Broer, D. J.; Feringa, B. L. Rotational Reorganization of Doped Cholesteric Liquid Crystalline Films. J. Am. Chem. Soc. 2006, 128, 14397−14407. (f) Eelkema, R.; Pollard, M. M.; Vicario, J.; Katsonis, N.; Ramon, B. S.; Bastiaansen, C. W. M.; Broer, D. J.; Feringa, B. L. Molecular Machines: Nanomotor Rotates Microscale Objects. Nature 2006, 440, 163. (13) (a) Astumian, R. D. Thermodynamics and Kinetics of a Brownian Motor. Science 1997, 276, 917−922. (b) Astumian, R. D.; Derenyi, I. A Chemically Reversible Brownian Motor: Application to Kinesin and NCD. Biophys. J. 1999, 77, 993−1002. (14) (a) Seldenthuis, J. S.; Prins, F.; Thijssen, J. M.; van der Zant, H. S. J. An All-Electric Single-Molecule Motor. ACS Nano 2010, 4, 6681− 6686. (b) Neumann, J.; Gottschalk, K. E.; Astumian, R. D. Driving and Controlling Molecular Surface Rotors with a Terahertz Electric Field. ACS Nano 2012, 6, 5242−5248. (15) (a) Kelly, T. R.; Cai, X.; Damkaci, F.; Panicker, S. B.; Tu, B.; Bushell, S. M.; Cornella, I.; Piggott, M. J.; Salives, R.; Cavero, M.; Zhao, Y.; Jasmin, S. Progress toward a Rationally Designed, Chemically Powered Rotary Molecular Motor. J. Am. Chem. Soc. 2007, 129, 376−386. (b) Kelly, T. R.; De, S. H.; Silva, R. A. Unidirectional Rotary Motion in a Molecular System. Nature 1999, 401, 150−2. (16) Rivado-Casas, L.; Sampedro, D.; Campos, P. J.; Fusi, S.; Zanirato, V.; Olivucci, M. Fluorenylidene−Pyrroline Biomimetic Light-Driven Molecular Switches. J. Org. Chem. 2009, 74, 4666−4674. (17) (a) Pijper, D.; van Delden, R. A.; Meetsma, A.; Feringa, B. L. Acceleration of a Nanomotor: Electronic Control of the Rotary Speed of a Light-Driven Molecular Rotor. J. Am. Chem. Soc. 2005, 127, 17612−17613. (b) ter Wiel, M. K. J.; van Delden, R. A.; Meetsma, A.; Feringa, B. L. Increased Speed of Rotation for the Smallest LightDriven Molecular Motor. J. Am. Chem. Soc. 2003, 125, 15076−15086. (18) (a) Amatatsu, Y. Theoretical Design of a Light-Driven Molecular Rotary Motor with Low Energy Helical Inversion: 9-(5- Methyl-2-phenyl-2-cyclopenten-1-ylidene)-9H-fluorene. J. Phys. Chem. A 2011, 115, 13611−13618. (b) Amatatsu, Y. Theoretical Design of a Fluorene-Based Light-Driven Molecular Rotary Motor with Constant Rotation. J. Phys. Chem. A 2012, 116, 10182−10193. (19) (a) Sampedro, D.; Migani, A.; Pepi, A.; Busi, E.; Basosi, R.; Latterini, L.; Elisei, F.; Fusi, S.; Ponticelli, F.; Zanirato, V.; Olivucci, M. Design and Photochemical Characterization of a Biomimetic LightDriven Z/E Switcher. J. Am. Chem. Soc. 2004, 126, 9349−9359. (b) Sinicropi, A.; Martin, E.; Ryazantsev, M.; Helbing, J.; Briand, J.; Sharma, D.; Leonard, J.; Haacke, S.; Cannizzo, A.; Chergui, M.; Zanirato, V.; Fusi, S.; Santoro, F.; Basosi, R.; Ferre, N.; Olivucci, M. An Artificial Molecular Switch That Mimics the Visual Pigment and Completes Its Photocycle in Picoseconds. Proc. Natl. Acad. Sci. U.S.A. 2008, 105, 17642−17647. (c) Lumento, F.; Zanirato, V.; Fusi, S.; Busi, E.; Latterini, L.; Elisei, F.; Sinicropi, A.; Andruniow, T.; Ferre, N.; Basosi, R.; Olivucci, M. Quantum Chemical Modeling and Preparation of a Biomimetic Photochemical Switch.

Angew. Chem., Int. Ed. 2007, 46, 414−420. (d) Bonacic-Koutecky, V.; Koehler, J.; Michl, J. Prediction of Structural and Environmental Effects on the S1−S0 Energy Gap and Jump Probability in Double-Bond cis−trans Photoisomerization. A General Rule. Chem. Phys. Lett. 1984, 104, 440−443. (e) Bonacic-Koutecky, V.; Koutecky, J.; Michl, J. Neutral and Charged Diradicals, Zwitterions, Funnels on the S1 Hypersurface and Proton Translocation; Their Importance for the Optical Process and Other Photochemical and Photophysical Processes. Angew. Chem. 1987, 99, 216−236. (20) The vibrational excess is calculated as the energy difference from the S3 vertical absorption (Franck−Condon region) to the current point considered on the potential energy surface. (21) (a) Garavelli, M.; Celani, P.; Bernardi, F.; Robb, M. A.; Olivucci, M. The C5H6NH2 + Protonated Schiff Base: An Ab Initio Minimal Model for Retinal Photoisomerization. J. Am. Chem. Soc. 1997, 119, 6891−6901. (b) Leonard, J.; Schapiro, I.; Briand, J.; Fusi, S.; Rossi Paccani, R.; Olivucci, M.; Haacke, S. Mechanistic Origin of the Vibrational Coherence Accompanying the Photoreaction of Biomimetic Molecular Switches. Chem.Eur. J. 2012, 18, 15296−15304. (22) Frutos, L. M.; Andruniow, T.; Santoro, F.; Ferre, N.; Olivucci, M. Tracking the Excited-State Time Evolution of the Visual Pigment with Multiconfigurational Quantum Chemistry. Proc. Natl. Acad. Sci. U.S.A. 2007, 104, 7764−7769. (23) (a) Schoenlein, R. W.; Peteanu, L. A.; Mathies, R. A.; Shank, C. V. The First Step in Vision: Femtosecond Isomerization of Rhodopsin. Science 1991, 254, 412−415. (b) Wang, Q.; Schoenlein, R. W.; Penteanu, L. A.; Mathies, R. A.; Shank, C. V. Vibrationally Coherent Photochemistry in the Femtosecond Primary Event of Vision. Science 1994, 266, 422−424. (24) Finley, J.; Malmqvist, P.-A.; Roos, B. O.; Serrano-Andres, L. The Multi-State CASPT2 Method. Chem. Phys. Lett. 1998, 288, 299−306. (25) The DC vector measures the distortion of the system providing the maximum coupling between the electronic states involved in the crossing. The GD vector measures the distortion of the system leading to the largest variation of the energy difference between the two electronic states involved in the crossing. (26) Aquilante, F.; De Vico, L.; Ferre, N.; Ghigo, G.; Malmqvist, P.- a.; Neogrady, P.; Pedersen, T. B.; Pitonak, M.; Reiher, M.; Roos, B. O.; Serrano-Andres, L.; Urban, M.; Veryazov, V.; Lindh, R. MOLCAS 7: The Next Generation. J. Comput. Chem. 2010, 31, 224−247. (27) Frisch, M. J.; Trucks, G. W.; Schlegel, H. B.; Scuseria, G. E.; Robb, M. A.; Cheeseman, J. R.; Scalmani, G.; Barone; V.; et al. Gaussian 09, revision B.01; Gaussian, Inc.: Wallingford, CT, 2009. (28) The branching plane is the plane spanned by the nonadiabatic coupling vectors (i.e., gradient difference and derivative coupling vectors) where energy degeneracy between the crossing states is left. (29) (a) Dartnall, H. J. The Visual Pigment of the Green Rods. Vision Res. 1967, 7, 1−16. (b) Burghardt, I.; Hynes, J. T. Excited-State Charge Transfer at a Conical Intersection: Effects of an Environment. J. Phys. Chem. A 2006, 110, 11411−11423. (c) Rivado-Casas, L.; Blanco-Lomas, M.; Campos, P. J.; Sampedro, D. Photochemical Characterization of Biomimetic Molecular Switches. Tetrahedron 2011, 67, 7570−7574. (30) Garavelli, M.; Bernardi, F.; Olivucci, M.; Vreven, T.; Klein, S.; Celani, P.; Robb, M. A. Potential-Energy Surfaces for Ultrafast Photochemistry: Static and Dynamic Aspects. Faraday Discuss. 1998, 110, 51−70. (31) (a) Tully, J. C. Molecular Dynamics with Electronic Transitions. J. Chem. Phys. 1990, 93, 1061−1071. (b) Craig, C. F.; Duncan, W. R.; Prezhdo, O. V. Trajectory Surface Hopping in the Time-Dependent Kohn−Sham Approach for Electron−Nuclear Dynamics. Phys. Rev. Lett. 2005, 95, 163001/1−163001/4. (c) Jaeger, H. M.; Fischer, S.; Prezhdo, O. V. Decoherence-Induced Surface Hopping. J. Chem. Phys. 2012, 137, 22A545/1−22A545/14. (32) Granucci, G.; Persico, M. Critical Appraisal of the Fewest Switches Algorithm for Surface Hopping. J. Chem. Phys. 2007, 126, 134114−134125. (33) Code implemented by

Valentini, A.; Frutos, L.M. working with MOLCAS 7.6 (see ref 26) CASSCF wave functions and energies. (34) Initial conditions were obtained by sampling the phase space for the minimum-energy structure on S0 with 1 ns dynamics. The dynamics were performed using a Nose− Hoover chain of thermostats with T = 300K (see the Supporting Information for additional details).